coatings

MDPI

Article

Tunable Coefficient of Thermal Expansion of Composite Materials for Thin-Film Coatings

Xu Long [1,*], Tianxiong Su [1], Zubin Chen [1], Yutai Su [1,*] and Kim S. Siow [2]

[1] School of Mechanics, Civil Engineering and Architecture, Northwestern Polytechnical University, Xi'an 710072, China; stx@mail.nwpu.edu.cn (T.S.); zb.chen@mail.nwpu.edu.cn (Z.C.)
[2] Institute of Microengineering and Nanoelectronics, Universiti Kebangsaan Malaysia, Bangi 43600, Malaysia; kimsiow@ukm.edu.my
* Correspondence: xulong@nwpu.edu.cn (X.L.); suyutai@nwpu.edu.cn (Y.S.)

Abstract: In most engineering applications, the coefficients of thermal expansion (CTEs) of different materials in integrated structures are inconsistent, especially for the thin-film multilayered coatings. Therefore, mismatched thermal deformation is induced due to temperature variation, which leads to an extreme temperature gradient, stress concentration, and damage accumulation. Controlling the CTEs of materials can effectively eliminate the thermally induced stress within the layered structures and thus considerably improve the mechanical reliability and service life. In this paper, randomly distributed fibers are incorporated into the matrix material and thus utilized to tune the material CTE from the macroscopical viewpoint. To this end, finite element (FE) modeling is proposed for fiber-reinforced matrix composites. In order to overcome the challenges of creating numerical models at a mesoscale, the random distribution of fibers in three-dimensional space is realized by proposing a fiber growth algorithm with the control of the in-plane and out-of-plane angles of fibers. The homogenization method is adopted to facilitate the FE simulations by using the representative volume element (RVE) of composite materials. Periodic boundary conditions (PBC) are applied to realize the prediction of the equivalent CTE of macroscopic composite materials with randomly distributed fibers. In the established FE model, the random distribution of carbon fibers in the matrix makes it possible to tune the CTE of the composite material by considering the orientation of fibers in the matrix. The FE predictions show that the volume fraction of carbon fibers in the composite materials is found to be crucial to macroscopic CTE, but results in minor variations in Young's modulus and shear modulus. With the developed ABAQUS plug-in program, the proposed tuning method for CTE is promising to be standardized for industrial practice.

Keywords: fiber-reinforced composite; finite element simulation; coefficient of thermal expansion; representative volume element; periodic boundary conditions

check for updates

Citation: Long, X.; Su, T.; Chen, Z.; Su, Y.; Siow, K.S. Tunable Coefficient of Thermal Expansion of Composite Materials for Thin-Film Coatings. *Coatings* **2022**, *12*, 836. https://doi.org/10.3390/coatings12060836

Academic Editors: Adrian David and Sergey N. Grigoriev

Received: 3 May 2022
Accepted: 13 June 2022
Published: 15 June 2022

1. Introduction

Fiber-reinforced matrix materials are composite materials formed by using fiber or carbon fiber fabric as reinforcement and resin, ceramic, metal, and cement as the matrix. Such composite materials have the advantages of convenient processing, high specific strength, and low relative density [1–3]. Such composite materials have been widely applied in various sectors of industries. As the core competency, the design and optimization of composite materials have been attracting more attention in scientific research and technological development. For fiber-reinforced matrix composites, it is important to understand the relationship between the macroscopic mechanical properties and the material microstructure. With the significant advance in computing capacity in recent years, numerical simulations can be performed for composite materials with increasingly complex microstructures, providing new ideas for the design of composite materials [4–6]. Based on the characteristics of fiber-reinforced matrix composites, it is difficult to accurately describe the mechanical properties of composites by traditional mechanical models at the macroscopic scale. Therefore, Panin [7] proposed the concept of micromechanics, which was also accepted by most scientific and technological workers. The advantage of this concept is that composite materials can be divided into multiple scale levels and analyzed individually. On the basis of Panin, Mishnaevsky [8] introduced the concept of mesoscopic continuum mechanics and concluded that this method also involves statistical principles and quantum mechanics.

With the rapid development of electronic packaging technology, chips are developing in the direction of miniaturization and high power. These all put forward higher requirements on the mechanical properties of packaging materials [9,10]. On this basis, some studies have been carried out on the influence of fiber materials on solder joints [11,12]. As the thermal effect continues to expand, the thermal failure problem of composite materials for thin-film coatings in the interconnect material in the package structure is also more serious. However, the current study on the coefficients of thermal expansion (CTEs) of composite materials for thin-film coatings still has great challenges.

Carbon-fiber-reinforced matrix composites have the advantages of high strength and isotropic elastic modulus, which are widely utilized in a wide range of applications such as aerospace and electronic packaging. However, fiber-reinforced materials are complex in their spatial configuration so far. Despite the extremely high randomness of the material at the mesoscopic level, it generally exhibits good property homogeneity at the macroscopic level. At appropriate geometrical scales, this localized inhomogeneity of the material can be manipulated and handled by mesoscale units, which are usually referred to as unit cells. In fact, there are a number of theoretical models and numerical methods for predicting the mechanical properties of carbon-fiber-reinforced composites. When performing calculations using mesomechanical models, Andriyana [13] considered not only the random distribution process of fibers but also the orientation of fibers. Wan and Takahashi [14] studied the effect of fiber aspect ratio on the tensile properties of materials by different modeling methods and obtained the fiber aspect ratio to achieve the best tensile properties based on the Mori–Tanaka model. However, it should be noted that the preparation process of carbon-fiber-reinforced composites is complicated, and there is an unaffordable number of variables involved in the preparation process. This leads to high research and development costs. Therefore, computer-aided design has been used to optimize the distribution and aspect ratio of fibers.

Mirkhalaf [15] carried out model design and nonlinear calculation using the reinforced matrix composite material module in the finite element (FE) software, and obtained the effects of different fiber volume fractions, fiber length–diameter ratios and orientation distributions on the macroscopic mechanical properties of composite material. Similarly, by using the Digimat-FE, Díaz [16] investigated the thermal conductivity of wood and Trzepieciński [17] completed the studies on the failure characteristics of composite materials. In addition, Chao et al. [18] found that chopped carbon fibers also have the characteristics of a negative thermal expansion coefficient in a certain direction. However, in the field of electronic packaging, there are few related studies on the contribution of carbon fibers to the mechanical properties of thin-film coating materials and the coefficient of thermal expansion of composites. Therefore, this paper investigates the tunable thermal expansion coefficient of composite materials for thin film coating.

In this study, a three-dimensional mesomechanical model of fiber-reinforced materials is developed by using the parameterized preprocess in ABAQUS. In this process, the application of the random distribution of carbon fibers in composites is realized through the secondary development script of the ABAQUS software, and the randomness of the direction of carbon fibers is included at the same time. In order to more deeply reveal the effect of carbon fiber microscale on the macroscopic mechanical properties of composites, the macroscopical coefficients of thermal expansion (CTEs) of carbon-fiber-reinforced matrix composites are calculated by using the representative volume element (RVE) method. Furthermore, the influence of the volume fraction of chopped carbon fibers on the macroscopic

CTE based on the RVE responses is explored, and it also provides a more reliable basis for the in-depth research and comprehensive application of thin-film coating materials. Accordingly, the study contents of this paper can be outlined as follows:

1. A simulation model of RVEs is established based on the theory of mesomechanics, and the process and difficulties of its establishment are described in detail.
2. The random distribution of the position and direction of the fiber material in the composite materials for thin-film coatings is realized by the calculation method combined with the relevant development script file of ABAQUS.
3. The close integration of periodic boundary condition theory and finite element simulation software is realized, and constraints are imposed on the corresponding nodes of the RVEs.
4. The macroscopic mechanical properties and CTE in RVEs are calculated based on the randomness of the fiber distribution.

Finally, the trend in the linear elastic properties and the CTE of the composites with fiber volume fraction are further analyzed, and it is found that there is a certain negative correlation, that is, with the increase in fiber volume fraction, the elastic modulus, shear modulus and CTE decrease gradually.

2. Modeling of Representative Volume Elements for Composite Materials

To perform efficient FE modeling for the fiber-reinforced matrix composites, the homogenization modeling approach is proposed on the basis of RVEs for analyzing the mesoscale mechanical properties of composites [19–22]. To represent the macroscopic material behavior and scale down the computational cost, periodic boundary conditions are applied on the RVE as well. Therefore, the equivalent CTE of the composites can be tuned through the adjustment of fiber properties [23–25]. In particular, the establishment of FE models involves the characteristics of the random distribution of fibers in the matrix and also considers the orientation of fibers inside the matrix, which is also a difficulty in establishing a mesomechanical model.

The mechanical properties of fiber-reinforced composites, including but not limited to the equivalent elastic properties, CTE, and volume fraction of fibers, can be investigated efficiently using RVE [26–28]. However, for composite materials with internally structured and randomly distributed fibers, it is important to reduce the computational cost by sensibly selecting numerical models, which should also be as large as possible by taking full account of the interaction between fibers and the matrix material. Thus, using a mesoscale RVE approach ensures both computational accuracy and efficiency. In order to adequately balance these contradictions, a mesomechanical approach is adopted in this paper to create three-dimensional numerical models of random fiber-reinforced matrix composites.

2.1. Representative Volume Element Design Steps

Traditional methods of designing fiber-reinforced matrix composites suffer from time-consuming design cycles and high manufacturing cost, which limit the efficiency of updating and iterating composites. This section realizes the rapid modeling of fiber-reinforced matrix composites through a Python program script file based on ABAQUS. On this basis, the influence of the material properties and geometric dimensions of the fibers and the matrix on the equivalent thermal expansion coefficient is studied.

In order to accurately simulate the distribution of three-dimensional fiber units in the matrix, the random distribution of fibers in the matrix is simulated according to the microstructure characteristics of fiber-reinforced matrix composites. Through the random generation algorithm, the initial coordinates of the fibers are determined, and the collective growth process of the fibers is determined by the placement algorithm. Based on this fiber placement algorithm, the accuracy of fiber placement can be significantly improved and the time required for model creation is reduced. When using the Python program script file to generate the model, the following issues should be paid attention to. The spatial position of the fiber inside the matrix usually includes fiber spatial coordinates, fiber radius, fiber length, fiber spatial orientation, and fiber-to-fiber distance judgment. Based on the above problems, using the Python program script based on ABAQUS, the creation process of RVEs of fiber-reinforced matrix composites in ABAQUS can be divided into the following five steps.

Step 1: Creation of a single fiber

As the fiber units are all solid units with the same radius and length, a fiber unit is first generated, and a specific number of fiber aggregates can be obtained by repeatedly repeating the operation. The resulting single fiber element is a solid element with a radius of 1.5 µm and a length of 10 µm.

Step 2: Generation process of fiber starting point coordinates

Generating a randomly distributed fiber usually includes the following parameters: the coordinates of the center of the fiber base, the radius of the fiber base, the total fiber length, and the fiber spatial orientation. Therefore, according to the uniform distribution of fibers in space, the function library of ABAQUS is used to generate a specific number of random numbers within a limited spatial range. Each group of random numbers represents the coordinates of the starting point of the fiber. The spatial distribution problem in the actual fiber formation process can be better simulated through this method, as shown in Figure 1.

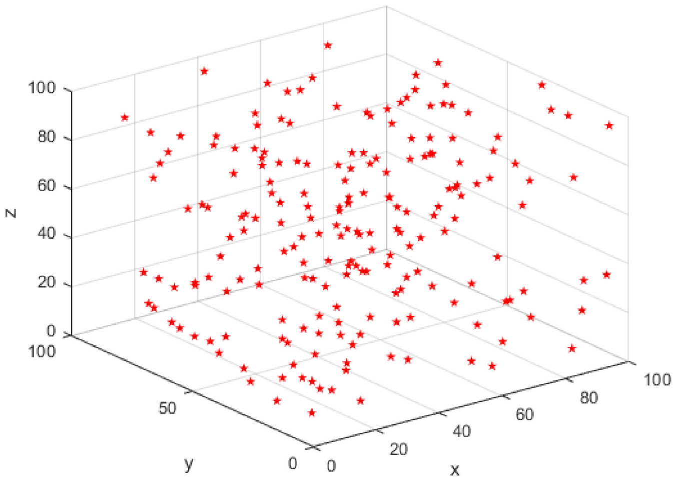

Figure 1. Three-dimensional coordinates of fibers randomly distributed in space.

Step 3: Generation process of fiber endpoint coordinates.

Assuming that the fiber is straight in the actual production process and the fiber does not bend during the growth process, the difference between the ending coordinate of the fiber and the starting coordinate of the fiber is the length and the spatial orientation value of the fiber. When a fiber rotates in three-dimensional space, it contains two parameters: the in-plane angle θ of the fiber, and the out-of-plane angle φ, as shown in Figure 2.

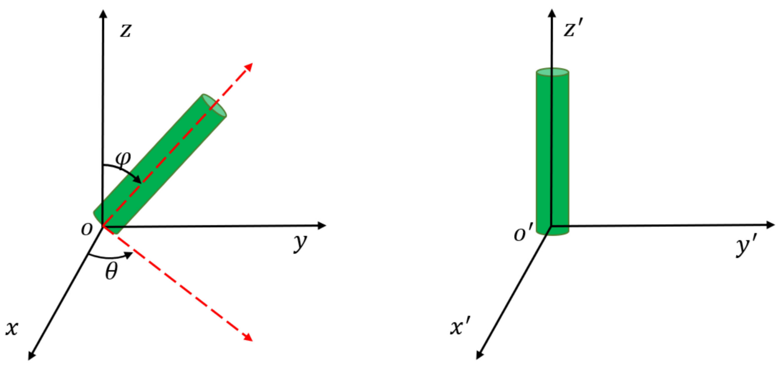

Figure 2. Angle parameter of fiber distribution in space.

The values of the spatial angles θ and φ of the fibers are randomly selected in the range of [0, 2π] to ensure that the generated overall fibers have macroscopic isotropic properties in statistics. In order to further study the probability distribution of fiber orientation in space, a second-order tensor A_{ij} was introduced, which was decomposed into the product of eigenvalues and eigenvectors, and represented as a three-dimensional ellipse in space, as shown in Figure 3.

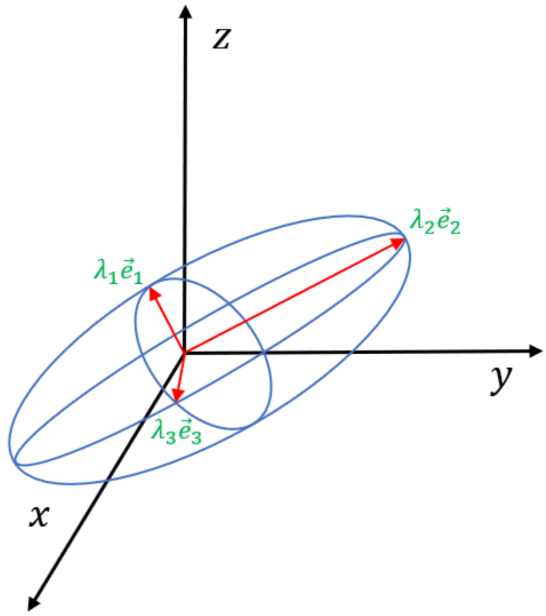

Figure 3. Definition of fiber orientation in three-dimensional space.

The direction vector formed from the center of the circle to any point on the ellipsoid can represent the distribution probability of the spatial fiber at this point. The direction distribution of each fiber is expressed by the angles θ and φ; then, the fiber distribution within a specific range can be expressed by

$$a_{ij} = \begin{bmatrix} sin^2\theta cos^2\theta & sin^2\theta sin\theta cos\varphi & sin\theta cos\theta cos\varphi \\ sin^2\theta sin\varphi cos\varphi & sin^2\theta sin^2\varphi & sin\varphi sin\theta cos\theta \\ cos\varphi sin\theta cos\theta & sin\varphi sin\theta cos\theta & sin^2\theta \end{bmatrix} \tag{1}$$

where a_{ij} is the orientation distribution, and through the above coordinate analysis and the analysis of fiber orientation in the fiber space, M and N can be used to represent the starting and end coordinates of the fiber; then, the starting point coordinates $M(M_x,\ M_y,\ M_z)$ and the end point $N(N_x,\ N_y,\ N_z)$ can be expressed as

$$\begin{aligned} M_x &= random.rand(a,b) \\ M_y &= random.rand(a,b) \\ M_z &= random.rand(a,b) \end{aligned} \tag{2}$$

$$\begin{aligned} N_x &= random.rand(a,b) + Lsin\varphi cos\theta \\ N_y &= random.rand(a,b) + Lsin\varphi sin\theta \\ N_z &= random.rand(a,b) + Lcos\varphi \end{aligned} \tag{3}$$

where θ is the in-plane angle, φ is the out-of-plane angle, L is the length of the fiber, a is the left boundary of the coordinate distribution, b is the right boundary of the coordinate, and *random* is the random distribution function inline in Python. According to Equations (2) and (3), the coordinates of the starting and end points of the fiber are determined, and the radius parameter R of the fiber is added to determine the relative position of the entire fiber inside the matrix.

Step 4: Interference determination of fibers based on spatial distance.

Since the starting point and end point coordinates of fibers are randomly generated, the phenomenon of fiber intersection inevitably occurs, and interference determination is required when the spatial position of the fiber is finally determined. When the phenomenon of fiber intersection occurs, the distribution law of fibers in the matrix cannot be well simulated, and also the intersected fibers lead to contact problems resulting in numerical divergence and also significantly increasing computational time. Therefore, in FE simulations, when the three-dimensional model of the fiber-reinforced matrix composite material is finally generated, it is also necessary to check the interference between the fibers.

The method of checking fiber interference is to determine the shortest distance between the centerlines of each fiber, which is usually greater than the diameter of the fiber's bottom surface. The center line of the fiber is a straight line in space, and the shortest distance between the two straight lines in space is the length of the common perpendicular. However, this paper needs to determine the shortest distance between the two lines in space, even if the distance of the common perpendicular is smaller than the fiber diameter. If the distance between the two ends of the fiber is ensured to be greater than the diameter, the fiber that meets the requirements may also be generated, as shown in Figure 4.

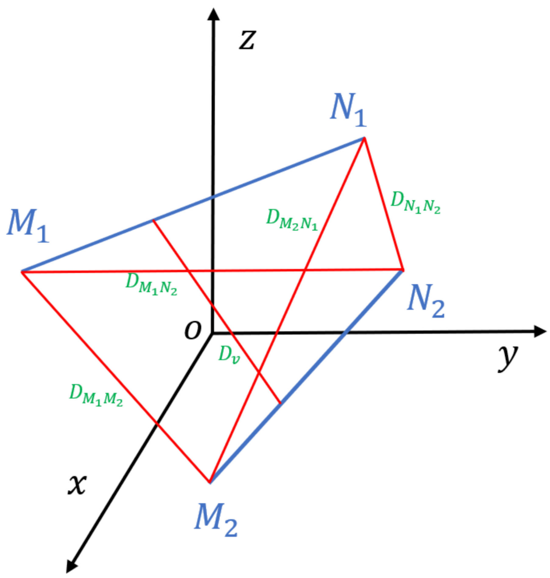

Figure 4. Determination of the distance between fibers.

When calculating the shortest distance between M_1N_1 and M_2N_2 of interspace line, it is necessary to obtain the common perpendicular line segment Dv of the different plane lines, and it is also necessary to calculate the lengths $D_{M_1M_2}$, $D_{M_1N_2}$, $D_{M_2N_1}$ and $D_{N_1N_2}$ of the lines between the four endpoints, and then compare with the diameter and length of the fiber, respectively, when D_v, $D_{M_1M_2}$, $D_{M_1N_2}$, $D_{M_2N_1}$ and $D_{N_1N_2}$ are smaller than the fiber diameter. It is determined that a fiber that meets the conditions has been generated, and the distance determination is calculated by

$$\begin{aligned} D_{M_1M_2} &= \sqrt{(M_{1x}-M_{2x})^2+\left(M_{1y}-M_{2y}\right)^2+(M_{1z}-M_{2z})^2} \\ D_{M_1N_2} &= \sqrt{(M_{1x}-N_{2x})^2+\left(M_{1y}-N_{2y}\right)^2+(M_{1z}-N_{2z})^2} \\ D_{M_2N_1} &= \sqrt{(M_{2x}-N_{1x})^2+\left(M_{2y}-N_{1y}\right)^2+(M_{2z}-N_{1z})^2} \\ D_{N_1N_2} &= \sqrt{(N_{1x}-N_{2x})^2+\left(N_{1y}-N_{2y}\right)^2+(N_{1z}-N_{2z})^2} \\ D_v &= \frac{\left|(\overrightarrow{M_1N_1}\times\overrightarrow{M_2N_2})\cdot\overrightarrow{M_1M_2}\right|}{\left|\overrightarrow{M_1N_1}\times\overrightarrow{M_2N_2}\right|} \end{aligned} \tag{4}$$

where $D_{M_1M_2}$ is the distance between points M_1 and M_2, $D_{M_1N_2}$ is the distance between points M_1 and N_2, $D_{M_2N_1}$ is the distance between points M_2 and N_1, $D_{N_1N_2}$ is the distance between points N_1 and N_2, and D_v is the distance between vertical line segments of interspace line M_1N_1 and M_2N_2.

Step 5: Generating fiber solid model based on ABAQUS python function library.

Through the script interface of ABAQUS, all the fiber space parameters that meet the requirements are processed into data and further reconstructed in ABAQUS, as shown in Figure 5. The reconstructed functions used can call the function library included in ABAQUS.

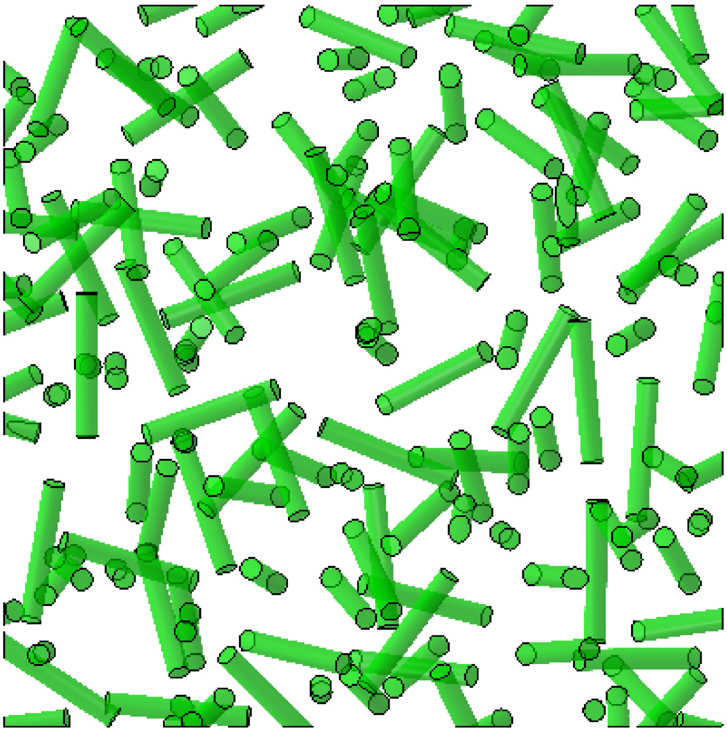

Figure 5. Randomly distributed fibers.

2.2. Periodic Boundary Conditions for the RVE

Fiber-reinforced matrix composites have local randomness. When using RVEs to carry out finite element numerical simulation of reinforced matrix composites, it is necessary to ensure the continuity between elements. There are three realization methods in numerical simulation to achieve this consistency on the boundary, given surface force, given displacement, and imposed periodic boundary conditions. However, for the model adopted in this paper, giving a surface force and displacement is unrealistic, so RVEs are applied in the periodic boundary conditions (PBC) [29]. In addition, Chen [30] applied each of the above boundary conditions using commercial FE software when investigating the equivalent mechanical properties of 2D porous materials and compared the final finite element analysis results with experiments. After comparison, it is found that when the PBC is applied to the representative element, the obtained FE analysis results are the closest to the actual properties of the material, and when the boundary conditions of a given surface force and a given displacement are used, the obtained finite element analysis results are obtained. There is often a large deviation in the numerical value between the analysis results and the real mechanical properties of the material. In addition, Chen et al. [30] also mentioned that if the real material model to be simulated has irregular shapes on the boundary surface, the real situation of the material can be more accurately predicted by using PBC by eliminating interfacial effects on irregular hole boundaries, as shown in Figure 6. Therefore, PBC is applied to the RVE boundary according to the research object and the above research results.

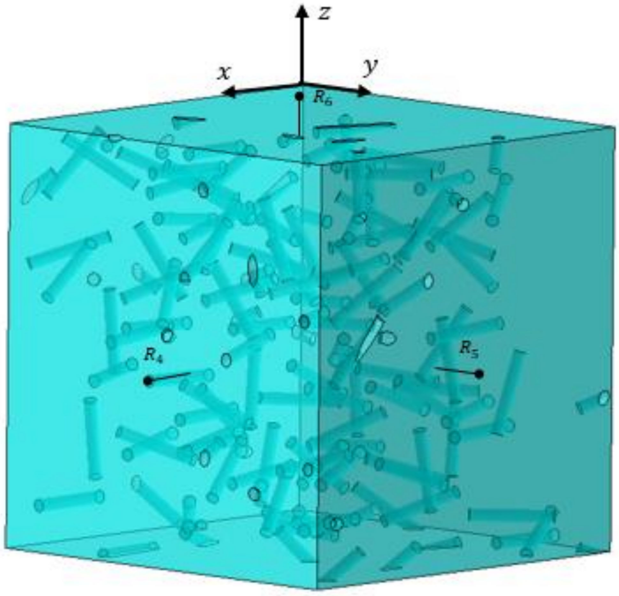

Figure 6. Schematic diagram of PBC for an RVE.

Based on the application method of periodic boundary conditions, deformation control can be performed on the boundary of RVEs so that the opposite surfaces of the elements have deformation compatibility. During the finite element simulation, each outer surface of the RVE has consistent deformation and force so that the entire fiber-reinforced matrix composite model conforms to the basic assumptions of continuum mechanics. The finite element analysis has laid the foundation. Suquet [31] conducted a theoretical derivation on the theory of periodic boundary conditions, and the specific derivation process can use the displacement field defined as Equation (5). In addition, Xia [32] completed further verification and application on this basis.

$$U_i = \bar{\varepsilon}_{ik} x_k + u_i^* \tag{5}$$

where $\bar{\varepsilon}_{ik}$ is the average strain of the representative volume unit, x_k is any position inside the representative volume unit, and u_i^* is the periodic displacement correction of the boundary position. The deformation coordination condition of Equation (5), u_i^*, is an unknown quantity in the deformation process, and is only related to the global load on the RVE, so this periodic displacement field cannot be applied to the actual operation process. In the fiber-reinforced matrix composite structure mentioned in this paper, the boundary surfaces of this structure are parallel so that the periodic displacement field can be written as

$$\begin{aligned} U_i^{j+} &= \bar{\varepsilon}_{ik} x_k^{j+} + u_i^* \\ U_i^{j-} &= \bar{\varepsilon}_{ik} x_k^{j-} + u_i^* \end{aligned} \tag{6}$$

where j^+ and j^- represent the positive and negative directions of the representative volume unit, respectively. Since in the periodic boundary condition, the value of u_i^* is the same on the two opposite surfaces, subtracting the displacement expressions on the left and right boundaries yields

$$U_i^{j+} - U_i^{j-} = \bar{\varepsilon}_{ik}(x_k^{j+} - x_k^{j-}) = \bar{\varepsilon}_{ik} \Delta x_k^j \tag{7}$$

where Δx_k^j is the relative displacement value of the relative boundary. For a specific $\bar{\varepsilon}_{ik}$, the displacement change on the right side of the above Equation is a constant, so the above equation can be rewritten as

$$u_i^{j+}(x, y, z) - u_i^{j-}(x, y, z) = c_i^j (i, j = 1, 2, 3) \tag{8}$$

By observing Equation (8), it can be found that the improved formula does not contain the correction amount of the periodic displacement. ABAQUS is used to impose periodic boundary conditions when the RVE is used for the simulation calculation. According to the above theoretical derivation process, more MPC point constraint equations are added to achieve stress–strain continuum conditions.

3. Equivalent CTE of Representative Volume Elements

This paper introduces three types of boundary conditions in finite element analysis. Among them, the displacement-based analysis conditions are natural boundary conditions, and the uniqueness of the solution is solved in the analysis process, but such boundary conditions cannot accurately describe the RVE in the stress–strain field induced during the deformation process. When applying periodic boundary conditions in ABAQUS, the grid nodes on the opposite surface can be used to control the application of MPC multipoint constraint equations. Most literature only mentions the mathematical expression of periodic boundary conditions and does not mention the realization process in ABAQUS finite element analysis, which is a considerable challenge for numerical analysis. This section mainly expounds on the theoretical basis and implementation methods of applying periodic boundary conditions in ABAQUS and then performs corresponding operations on the corresponding nodes, edge nodes, and vertices on the parallel plane of the RVE, as shown in Figure 7.

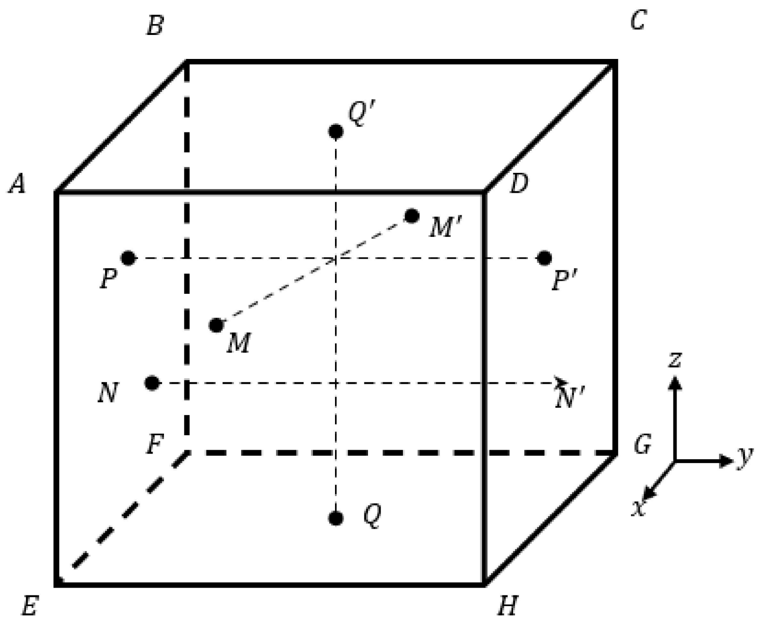

Figure 7. Boundary conditions for multipoint constraint equations.

In this paper, in the finite element software ABAQUS, the RVE is generated by the Python scripts. In addition, to ensure the consistency of the deformation of the symmetrical points and surfaces of the RVE, it is necessary to use the method of Python script files. The equivalent linear elastic mechanical properties of fiber-reinforced matrix composites will be studied later. The modeling process of the RVE of the fiber-reinforced matrix composite material in the finite element software was introduced in detail above. This paper adopts the finite element model method to calculate the equivalent linear elastic mechanical properties of the RVE. The method for calculating the equivalent linear elastic mechanical properties of RVEs in this paper is based on the ABAQUS plug-in program.

In this paper, the thermal expansion coefficient of the fiber-reinforced base needs to be regulated, so for the convenience of research, the elastic material properties of the selected two-phase materials are given in Tables 1 and 2.

Table 1. Material properties of reinforced fibers.

Elastic (GPa)	E_1 174	E_2 174	E_3 9.6	G_{12} 70.4	G_{13} 3.7	G_{23} 3.7	ν_{12} 0.234	ν_{13} 0.273	ν_{23} 0.273
CTE ($\times 10^{-6}$/K)		α_{11} -0.07044			α_{22} -0.07044			α_{33} 10.4956	

Table 2. Mechanical properties of the matrix material.

Material Name	Elastic Modulus (GPa)	Poisson's Ratio	α ($\times 10^{-6}$/K)
SAC305	20	0.4	24

Fiber is a transversely isotropic material. When calculating with ABAQUS, it is necessary to assign a local coordinate system to the material, and the thermal expansion coefficient of the fiber is also related to the direction.

According to the data in Table 2, fibers are regarded as transversely isotropic materials, each of which has an elastic axis of symmetry. The elastic constitutive relationship at any two positions with this axis as the axis of symmetry is all the same. Therefore, when a plane is perpendicular to the elastic symmetry axis, all directions in the plane are exactly symmetrical to the elastic symmetry axis, and the elastic constitutive relationship is the same. In transversely isotropic materials, the in-plane constitutive relation has in-plane isotropy. The typical representative in nature is the flaky distribution of rocks. In this paper, the elastic constitutive relation of the fibers in the isotropic plane is the same.

The elastic symmetry axis of the fiber is the radial direction of the fiber, so the direction of the Z axis is taken as the elastic symmetry axis of the fiber, and the coordinate axes X and Y establish an isotropic symmetry plane, as shown in Figure 8. In the isotropic symmetry plane, when the X and Y coordinates are exchanged, the elastic constitutive relation of the material does not change. In order to satisfy this condition, the elastic constitutive Jacobian matrix coefficient must satisfy

$$\begin{aligned} c_{11} &= c_{22} \\ c_{13} &= c_{23} \\ c_{55} &= c_{66} \end{aligned} \tag{9}$$

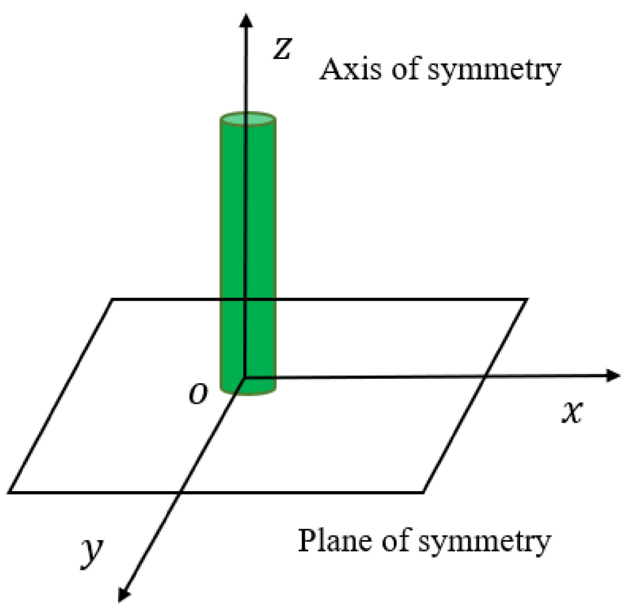

Figure 8. Elastic constitutive properties of fibers.

Additionally, according to the invariant principle of the shear stress–strain relationship given by:

$$c_{44} = \frac{1}{2}(c_{11} - c_{12}) \tag{10}$$

Through the above analysis, the elastic material properties of fibers can be described only by five independent elastic constants, and the elastic matrix of fibers can be written as

$$\begin{bmatrix} c_{11} & c_{12} & c_{13} & 0 & 0 & 0 \\ c_{12} & c_{11} & c_{13} & 0 & 0 & 0 \\ c_{13} & c_{13} & c_{13} & 0 & 0 & 0 \\ 0 & 0 & 0 & \frac{1}{2}(c_{11} - c_{12}) & 0 & 0 \\ 0 & 0 & 0 & 0 & c_{55} & 0 \\ 0 & 0 & 0 & 0 & 0 & c_{55} \end{bmatrix} \tag{11}$$

When using elastic parameters in ABAQUS, it also needs to be converted into a stiffness matrix. Invert Equation (11) to obtain Equation (12):

$$\begin{Bmatrix} \varepsilon_x \\ \varepsilon_y \\ \varepsilon_z \\ \gamma_{xy} \\ \gamma_{yz} \\ \gamma_{zx} \end{Bmatrix} = \begin{bmatrix} \frac{1}{E} & -\frac{\nu}{E} & -\frac{\nu'}{E} & 0 & 0 & 0 \\ -\frac{\nu}{E} & \frac{1}{E} & -\frac{\nu'}{E} & 0 & 0 & 0 \\ -\frac{\nu'}{E'} & -\frac{\nu'}{E'} & \frac{1}{E'} & 0 & 0 & 0 \\ 0 & 0 & 0 & \frac{1}{G} & 0 & 0 \\ 0 & 0 & 0 & 0 & \frac{1}{G'} & 0 \\ 0 & 0 & 0 & 0 & 0 & \frac{1}{G'} \end{bmatrix} \begin{Bmatrix} \sigma_x \\ \sigma_y \\ \sigma_z \\ \tau_{xy} \\ \tau_{yz} \\ \tau_{zx} \end{Bmatrix} \tag{12}$$

For transversely isotropic materials, the elastic axis of symmetry for each fiber needs to be defined in ABAQUS, as shown in Figure 9. However, the direction of each fiber is random. When the number of fibers reaches dozens or hundreds, how to accurately apply an elastic axis of symmetry to each fiber is a technical problem that needs to be solved urgently.

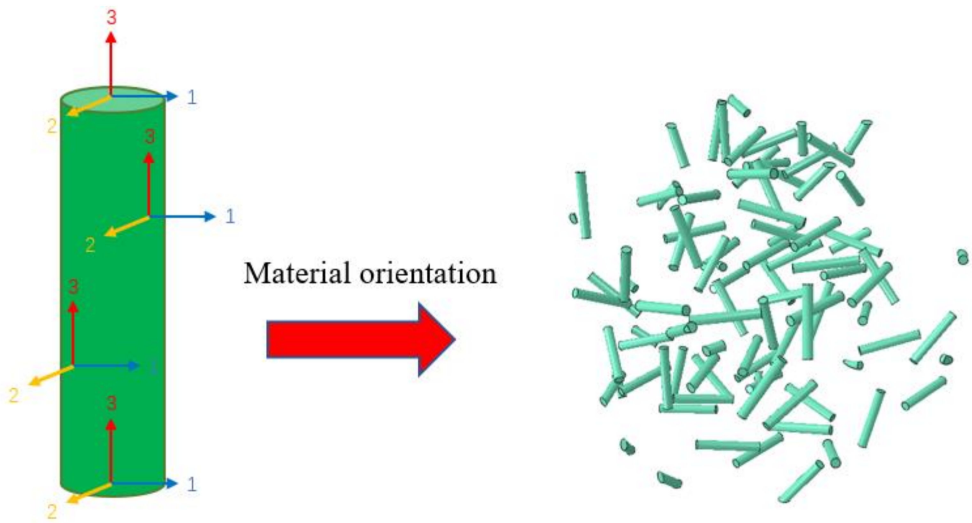

Figure 9. Material orientation of fibers.

In this paper, the Python script based on ABAQUS preprocessing is used to realize the assignment of the local coordinate system to all random fibers. In ABAQUS, a local coordinate system needs to be applied to each fiber first. For fibers, the application of the local coordinate system is often related to the bottom surface and bottom surface circumference of the fiber. The bottom surface is selected to define the isotropic surface of the fiber, and the bottom surface circumference is selected to define the elastic axis of symmetry of the fiber. Since the bottom surface and bottom surface circumference of each fiber are different, it is necessary to use the preprocessing script to define the set of bottom surface and bottom surface circumference each time random fibers are generated to lay the foundation for the subsequent automatic addition of material directions, as shown in Figure 10. Figure 10 highlights the local coordinate direction of each fiber in the model, and uses 1, 2, and 3 displayed in different colors to represent the three axes of x, y, and z of the spatial coordinate system.

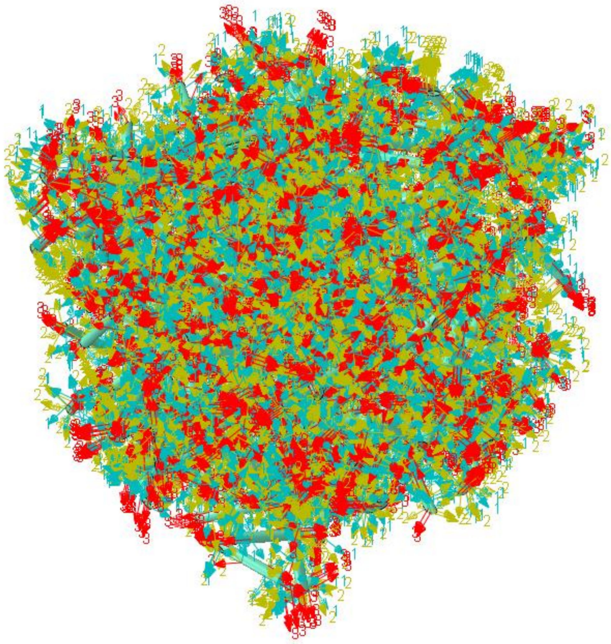

Figure 10. Schematic diagram of fiber local coordinate system definition.

Similar to the method by Chao [18], the fibers used in this paper have a negative thermal expansion coefficient on the isotropic plane and a positive thermal expansion coefficient in the radial direction of the fibers, which means that when the temperature increases, the shrinkage ratio of the fibers in the circumferential direction will be greater than the elongation ratio in the radial direction so that the overall control of the equivalent thermal expansion coefficient can be achieved. For the electronic packaging thin-film coating materials studied in this paper, the calculation is performed assuming that the base material is an isotropic material. Based on the above analysis process, this paper has studied the equivalent mechanical properties and thermal expansion coefficients of fiber-reinforced matrix composites with different volume fractions.

4. Result Discussion

In this paper, the generation method of fibers is to control the random generation number of the coordinates of the fiber starting point. During each iteration of the calculation, the different volume fraction of fibers can be easily generated by modifying the number of fibers in the model. The tetrahedral mesh is used in the generated finite element model, and the element type is C3D10, as shown in Table 3.

According to Table 3, as the number of iterations increases, the number of fibers increases steadily, increasing the volume fraction of fibers. Due to the strong randomness of the spatial distribution of fibers, the generated finite element model needs to be divided into many meshes. When the fiber volume fraction is close to 2%, it reaches more than 400,000 meshes, still in the mesh density. When more extensive, this presents a higher challenge to finite element calculation. Through finite element calculation, the data shown in Table 4 are obtained.

Table 3. Fiber integration in the generated finite element models.

Fiber Numbers	Volume Fraction	Mesh Number	Computing Time (s)
50	0.2356	149,560	430
100	0.4799	205,991	885
150	0.6646	255,566	1142
200	0.8695	302,956	1537
250	1.1039	320,125	1914
300	1.2512	348,464	2085
350	1.3916	348,464	2423
400	1.6425	367,355	2751
450	1.8191	398,205	3005
500	1.9704	412,653	3363

Table 4. Equivalent linear elastic mechanical properties of fiber-reinforced matrix composites.

Volume	0.23%	0.47%	0.66%	0.86%	1.10%	1.25%	1.39%	1.64%	1.81%	1.97%
E_1(GPa)	19.989	19.971	19.968	19.953	19.942	19.935	19.926	19.909	19.902	19.886
E_2(GPa)	19.988	19.974	19.965	19.955	19.942	19.933	19.926	19.913	19.899	19.895
E_3(GPa)	19.987	19.972	19.967	19.954	19.939	19.936	19.925	19.910	19.901	19.890
G_{12}(GPa)	7.819	7.804	7.784	7.771	7.765	7.751	7.737	7.722	7.712	7.705
G_{13}(GPa)	7.814	7.799	7.787	7.779	7.761	7.757	7.748	7.733	7.720	7.712
G_{23}(GPa)	7.812	7.803	7.787	7.776	7.769	7.756	7.753	7.736	7.726	7.721
ν_{12}	0.277	0.277	0.276	0.276	0.275	0.275	0.274	0.274	0.274	0.273
ν_{13}	0.278	0.277	0.277	0.276	0.276	0.275	0.274	0.274	0.274	0.273
ν_{23}	0.277	0.276	0.276	0.276	0.276	0.275	0.275	0.274	0.273	0.273

According to Table 4, the fibers act as a transversely isotropic material, but the phenomenon that makes the material properties of composites different in different directions is due to the fibers being distributed in the matrix according to the characteristics of random starting positions and random fiber orientations. In addition, with the continuous increase in the fiber volume fraction, the equivalent linear elastic mechanical properties of the composite show a decreasing trend. The values of E_1, E_2, and E_3 are very close, and it can be found that it can be approximated as a linear decrease. For the equivalent shear modulus of fiber-reinforced matrix materials, the numerical differences in the three planes are not large, and it can be approximately considered that with the increase in fiber volume fraction, the equivalent shear modulus approximately exhibits a linearly decreasing trend. The equivalent Poisson's ratios in the three principal planes do not change much and can be considered consistent. Therefore, the above-generated fiber-reinforced matrix composites can be regarded as isotropic materials, and the calculated stress distributions are shown in Figures 11 and 12.

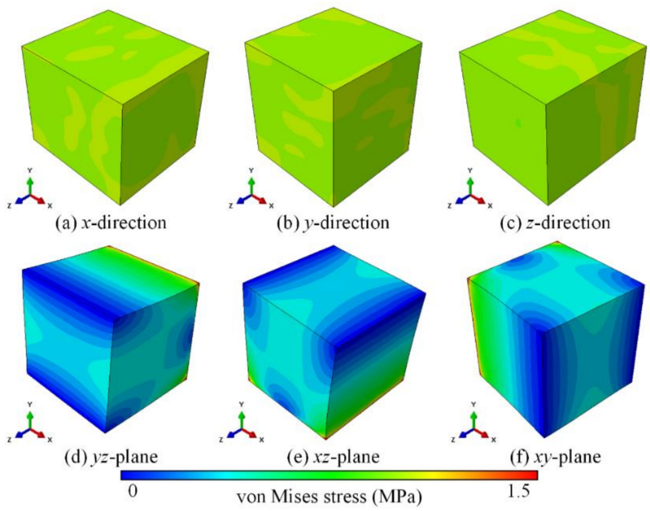

Figure 11. Equivalent linear elastic properties of RVEs.

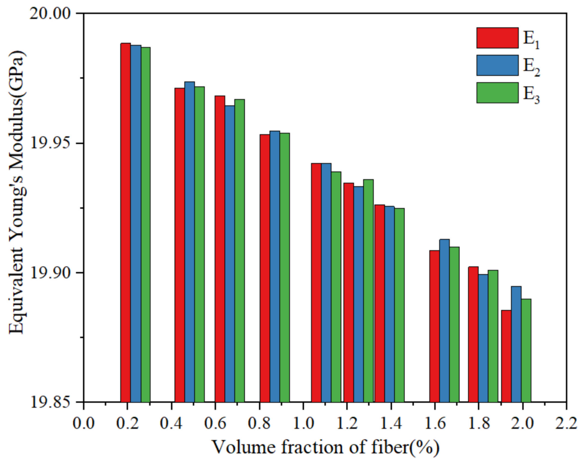

Figure 12. Variation trend in equivalent Young's modulus.

As shown in Figure 12, the equivalent moduli E_1, E_2, E_3 in the three planes are very close. When the volume fraction is 0, it is an isotropic material with an elastic modulus of 20 GPa. At the same time, it can be found that the values of E_1, E_2, and E_3 decrease linearly with the fiber volume fraction. After fitting the Origin data, Equation (13) can be obtained.

$$\begin{aligned} E_1 &= 20 - 0.055 \times Volum\_F \\ E_2 &= 20 - 0.053 \times Volum\_F \\ E_3 &= 20 - 0.054 \times Volum\_F \end{aligned} \tag{13}$$

where E_1, E_2, E_3 are three different equivalent linear elastic moduli, and $Volum\_F$ is the fiber volume fraction.

As shown in Figure 13, the equivalent shear modulus of the fibers in the three planes has approximately the same value. With the continuous increase in the fiber volume fraction, the equivalent shear modulus shows a linearly decreasing trend. The data fitting can obtain Equation (14):

$$\begin{aligned} G_{12} &= 7.833 - 0.066 \times Volum\_F \\ G_{13} &= 7.828 - 0.058 \times Volum\_F \\ G_{23} &= 7.825 - 0.054 \times Volum\_F \end{aligned} \tag{14}$$

where G_{12}, G_{13}, G_{23} are three different equivalent shear moduli, and $Volum\_F$ is the fiber volume fraction. In addition, the macroscopic thermal expansion coefficient of fiber-reinforced matrix composites needs to be analyzed, and the results are shown in Figure 14.

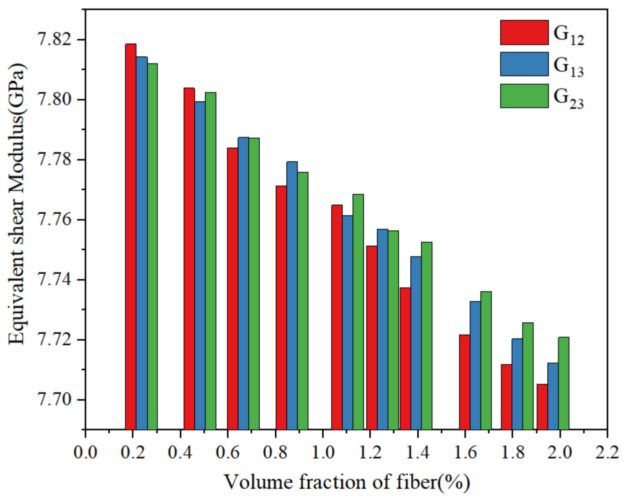

Figure 13. Variation trend in equivalent shear modulus.

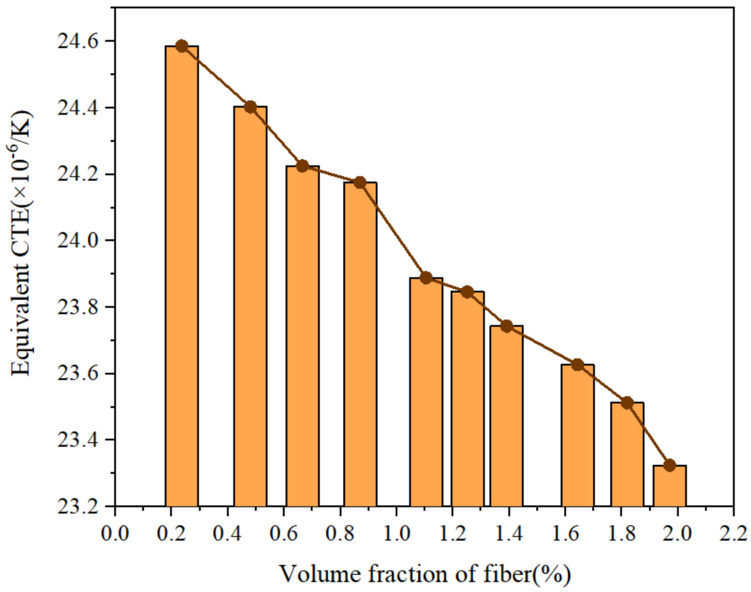

Figure 14. Trend in equivalent CTE with the variation in volume fraction of fibers.

It can be seen from that as the fiber content continues to increase, the equivalent thermal expansion coefficient of the representative volume unit continues to decrease. It can be seen from the numerical value that the overall thermal expansion coefficient decreases by a considerable amount, which is limited by the calculation cost and calculation accuracy. The highest content of fiber volume fraction discussed in this paper is close to 2%, and the empirical Equation (15) is obtained by linear fitting of Origin data:

$$\alpha_{eq} = 2.47267 \times 10^{-5} - 6.94244 \times 10^{-7} \times Volum\_F \tag{15}$$

where α_{eq} is the equivalent thermal expansion coefficient, $Volum\_F$ is the fiber volume fraction.

According to the change trends in the above calculation results, further analysis is completed and it is found that the reason for the equivalent Young's modulus and shear modulus showing linear decreasing trends as the volume fraction of the fibers increases is due to the linear elastic properties of the carbon fiber and base matrix material. Moreover, the different CTEs of the carbon fiber and matrix material cause the CTE of the thin-film coating material to change with the carbon fiber volume fraction. Additionally, the CTE of carbon fiber is much smaller than that of the matrix material, which also causes the CTE of the thin-film coating material to decrease with the increase in the carbon fiber volume fraction.

5. Conclusions

This paper mainly introduced the study on regulating the coefficient of thermal expansion of composite materials for thin-film coatings used in the field of electronic packaging. Based on the advantages of convenience, efficiency, and versatility of the commercial finite element software ABAQUS, numerical simulations of fiber-reinforced matrix composites were achieved by utilizing the representative volume element. Additionally, according to the theory of mesomechanics, periodic mesh division and the application of periodic boundary conditions were realized on the finite element model. Moreover, the equivalent linear elastic mechanical properties of composites were further studied, including the equivalent Young's modulus, equivalent shear modulus, and the variation law of the effective thermal expansion coefficient with the fiber volume fraction.

When the volume fraction of fibers accounts for 2% of the matrix, the Young's modulus of the fiber-reinforced matrix composite is adjusted to 19.886 GPa, the shear modulus is 7.7 GPa, and the equivalent thermal expansion coefficient is 23.324 ppm/K. The control effect of linear elastic mechanical properties is noticeable. This paper mainly has the following two conclusions:

1. The mesomechanical modeling of fiber-reinforced matrix composites is complex, involving the random distribution and random orientation of fibers. In this paper, the parametric modeling method based on Python program script files was used to improve modeling efficiency significantly.
2. Through the finite element analysis of the fiber-reinforced matrix composite material model, it was found that the equivalent thermal expansion coefficient of the material can be effectively reduced with the continuous increase in the fiber volume fraction.

Author Contributions: Conceptualization, X.L. and Y.S.; investigation, T.S. and Z.C.; writing—original draft preparation, X.L. and Z.C.; writing—review and editing, T.S., K.S.S. and Y.S.; funding acquisition, X.L.; supervision, X.L. All authors have read and agreed to the published version of the manuscript.

Funding: This work was supported by the National Natural Science Foundation of China (No. 52175148), the Natural Science Foundation of Shaanxi Province (No. 2021KW-25), the Open Cooperation Innovation Fund of Xi'an Modern Chemistry Research Institute (No. SYJJ20210409), and the Fundamental Research Funds for the Central Universities (No. 3102018ZY015).

Institutional Review Board Statement: Not applicable.

Informed Consent Statement: Not applicable.

Data Availability Statement: Not applicable.

Conflicts of Interest: The authors declare no conflict of interest.

References

1. Zeng, Q.; Yu, A.; Lu, G.M. Interfacial interactions and structure of polyurethane intercalated nanocomposite. *Nanotechnology* **2005**, *16*, 2757. [CrossRef]
2. Hashimoto, M.; Okabe, T.; Sasayama, T.; Matsutani, H.; Nishikawa, M. Prediction of tensile strength of discontinuous carbon fiber/polypropylene composite with fiber orientation distribution. *Compos. Part A Appl. Sci. Manuf.* **2012**, *43*, 1791–1799. [CrossRef]
3. Kwon, D.J.; Jang, Y.J.; Choi, H.H.; Kim, K.; Kim, G.H.; Kong, J.; Nam, S.Y. Impacts of thermoplastics content on mechanical properties of continuous fiber-reinforced thermoplastic composites. *Compos. Part B Eng.* **2021**, *216*, 108859. [CrossRef]
4. Lee, J.Y.; Baljon, A.; Loring, R.F.; Panagiotopoulos, A.Z. Simulation of polymer melt intercalation in layered nanocomposites. *J. Chem. Phys.* **1998**, *109*, 10321–10330. [CrossRef]
5. Smith, G.D.; Bedrov, D.; Li, L.W.; Byutner, O. A molecular dynamics simulation study of the viscoelastic properties of polymer nanocomposites. *J. Chem. Phys.* **2002**, *117*, 9478–9489. [CrossRef]
6. Thompson, R.B.; Ginzburg, V.V.; Matsen, M.W.; Balazs, A.C. Block copolymer-directed assembly of nanoparticles: Forming mesoscopically ordered hybrid materials. *Macromolecules* **2002**, *35*, 1060–1071. [CrossRef]
7. Panin, V.E. *Physical Mesomechanics of Heterogeneous Media and Computer-Aided Design of Materials*; Cambridge International Science Publishing: Cambridge, UK, 1998.
8. Mishnaevsky, L.L., Jr.; Schmauder, S. Contimuum mesomechanical finite element modeling in materials development: A state-of-the-art review. *Adv. Mech.* **2002**, *54*, 49.
9. Long, X.; Guo, Y.; Chang, X.; Su, Y.; Shi, H.; Huang, T.; Tu, B.; Wu, Y. Effect of Temperature on the Fatigue Damage of SAC305 Solder. In Proceedings of the 2021 22nd International Conference on Electronic Packaging Technology (ICEPT), Xiamen, China, 14–17 September 2021; pp. 1–4.
10. Long, X.; Su, T.; Chang, C.; Huang, J.; Chang, X.; Su, Y.; Shi, H.; Huang, T.; Wu, Y. Mechanical Behavior of Lead-Free Solder at High Temperatures and High Strain Rates. In Proceedings of the 2021 22nd International Conference on Electronic Packaging Technology (ICEPT), Xiamen, China, 14–17 September 2021; pp. 1–4.
11. Andriyana, A.; Billon, N.; Silva, L. Mechanical response of a short fiber-reinforced thermoplastic: Experimental investigation and continuum mechanical modeling. *Eur. J. Mech. A Solids* **2010**, *29*, 1065–1077. [CrossRef]
12. Wan, Y.; Takahashi, J. Tensile properties and aspect ratio simulation of transversely isotropic discontinuous carbon fiber reinforced thermoplastics. *Compos. Sci. Technol.* **2016**, *137*, 167–176. [CrossRef]
13. Mirkhalaf, S.M.; Eggels, E.H.; van Beurden, T.J.H.; Larsson, F.; Fagerström, M. A finite element based orientation averaging method for predicting elastic properties of short fiber reinforced composites. *Compos. Part B Eng.* **2020**, *202*, 108388. [CrossRef]
14. Díaz, A.R.; Flores, E.I.S.; Yanez, S.J.; Vasco, D.A.; Pina, J.C.; Guzmán, C.F. Multiscale modeling of the thermal conductivity of wood and its application to cross-laminated timber. *Int. J. Therm. Sci.* **2019**, *144*, 79–92. [CrossRef]

15. Trzepieciński, T.; Ryzińska, G.; Biglar, M.; Gromada, M. Modelling of multilayer actuator layers by homogenisation technique using Digimat software. *Ceram. Int.* **2016**, *43*, 3259–3266. [CrossRef]
16. Chao, X.J.; Qi, L.H.; Tian, W.L.; Lu, Y.F.; Li, H.J. Potential of porous pyrolytic carbon for producing zero thermal expansion coefficient composites: A multi-scale numerical evaluation. *Compos. Struct.* **2020**, *235*, 111819. [CrossRef]
17. Miller, W.; Hook, P.B.; Smith, C.W.; Wang, X.; Evans, K.E. The manufacture and characterisation of a novel, low modulus, negative Poisson's ratio composite. *Compos. Sci. Technol.* **2009**, *69*, 651–655. [CrossRef]
18. Sun, Z.; Shan, Z.D.; Shao, T.M.; Li, J.H.; Wu, X.C. A multiscale modeling for predicting the thermal expansion behaviors of 3D C/SiC composites considering porosity and fiber volume fraction. *Ceram. Int.* **2021**, *47*, 7925–7936. [CrossRef]
19. Wei, K.; Peng, Y.; Wang, K.Y.; Duan, S.Y.; Yang, X.J.; Wen, W.B. Three dimensional lightweight lattice structures with large positive, zero and negative thermal expansion. *Compos. Struct.* **2018**, *188*, 287–296. [CrossRef]
20. Liu, H.; Zeng, D.; Li, Y.; Jiang, L.Y. Development of RVE-embedded solid elements model for predicting effective elastic constants of discontinuous fiber reinforced composites. *Mech. Mater.* **2016**, *93*, 109–123. [CrossRef]
21. Kobayashi, S.; Shimpo, T.; Goto, K. Microscopic damage behavior in carbon fiber reinforced plastic laminates for a high accuracy antenna in a satellite under cyclic thermal loading. *Adv. Compos. Mater.* **2019**, *28*, 259–269. [CrossRef]
22. Hao, X.L.; Zhou, H.Y.; Mu, B.S.; Chen, L.; Guo, Q.; Yi, X.; Sun, L.C.; Wang, Q.W.; Ou, R.X. Effects of fiber geometry and orientation distribution on the anisotropy of mechanical properties, creep behavior, and thermal expansion of natural fiber/HDPE composites. *Compos. Part B Eng.* **2020**, *185*, 107778. [CrossRef]
23. Gu, J.P.; Leng, J.S.; Sun, H.Y.; Zeng, H.; Cai, Z.B. Thermomechanical constitutive modeling of fiber reinforced shape memory polymer composites based on thermodynamics with internal state variables. *Mech. Mater.* **2019**, *130*, 9–19. [CrossRef]
24. Sun, Q.P.; Zhou, G.W.; Meng, Z.X.; Jain, M.; Su, X.M. An integrated computational materials engineering framework to analyze the failure behaviors of carbon fiber reinforced polymer composites for lightweight vehicle applications. *Compos. Sci. Technol.* **2021**, *202*, 108560. [CrossRef]
25. Chen, L.L.; Gu, B.Q.; Zhou, J.F.; Tao, J.H. Study of the effectiveness of the RVEs for random short fiber reinforced elastomer composites. *Fibers Polym.* **2019**, *20*, 1467–1479. [CrossRef]
26. Naili, C.; Doghri, I.; Kanit, T.; Sukiman, M.S.; Aissa-Berraies, A.; Imad, A. Short fiber reinforced composites: Unbiased full-field evaluation of various homogenization methods in elasticity. *Compos. Sci. Technol.* **2020**, *187*, 107942. [CrossRef]
27. Garoz, D.; Gilabert, F.A.; Sevenois, R.D.B.; Spronk, S.W.F.; Van Paepegem, W. Consistent application of periodic boundary conditions in implicit and explicit finite element simulations of damage in composites. *Compos. Part B Eng.* **2019**, *168*, 254–266. [CrossRef]
28. Chen, L.; Tao, X.M.; Choy, C.L. Mechanical analysis of 3-D braided composites by the finite multiphase element method. *Compos. Sci. Technol.* **1999**, *59*, 2383–2391. [CrossRef]
29. Suquet, P. Elements of homogenization for inelastic solid mechanics. In *Homogenization Techniques for Composite Media*; Springer: Berlin/Heidelberg, Germany, 1987.
30. Xia, Z.H.; Zhang, Y.F.; Ellyin, F. A unified periodical boundary conditions for representative volume elements of composites and applications. *Int. J. Solids Struct.* **2003**, *40*, 1907–1921. [CrossRef]
31. Xia, Z.H.; Zhou, C.W.; Yong, Q.L.; Wang, X.W. On selection of repeated unit cell model and application of unified periodic boundary conditions in micro-mechanical analysis of composites. *Int. J. Solids Struct.* **2006**, *43*, 266–278. [CrossRef]
32. Xia, W.X.; Oterkus, E.; Oterkus, S. Ordinary state-based peridynamic homogenization of periodic micro-structured materials. *Theor. Appl. Fract. Mech.* **2021**, *113*, 102960. [CrossRef]